Ionics (2019) 25:2007–2016
https://doi.org/10.1007/s11581-018-2621-4

ORIGINAL PAPER

Effectively enhance high voltage stability of $LiNi_{1/3}Co_{1/3}Mn_{1/3}O_2$ cathode material with excellent energy density via La_2O_3 surface modified

Gang Sun [1,2] · Chenxiao Jia [1,2] · Jianning Zhang [1] · Wu Yang [1] · Zhipeng Ma [1] · Guangjie Shao [1,2] · Xiujuan Qin [1,2]

Received: 8 April 2018 / Revised: 31 May 2018 / Accepted: 4 June 2018 / Published online: 15 June 2018

Abstract

La_2O_3-coated $LiNi_{1/3}Mn_{1/3}Co_{1/3}O_2$ has been successfully synthesized via a wet chemical process followed. The 3 wt% La_2O_3-coated $LiNi_{1/3}Mn_{1/3}Co_{1/3}O_2$ illustrated highest rate capability, lowest voltage decay, outstanding cycling performance, and excellent energy density at the range of 2.5–4.5 V. The discharge capacity of $LiNi_{1/3}Mn_{1/3}Co_{1/3}O_2$ at a 5C rate increases from 86.9 to 137.5 mA h g^{-1} upon coating with La_2O_3 particles. The decrements of the average discharge voltages for 3 wt% La_2O_3-coated $LiNi_{1/3}Mn_{1/3}Co_{1/3}O_2$ electrode is 10.3 mV over 100th cycle and 26.9 mV over 200th cycle compared to 407 mV over 100th cycle for bare nickel cobalt manganese. The energy densities retention of 3 wt% La_2O_3-coated $LiNi_{1/3}Mn_{1/3}Co_{1/3}O_2$ is 96.5% after 100 cycles and 89.7% after 200 cycles compared to 34.5% after 100 cycles for bare $LiNi_{1/3}Mn_{1/3}Co_{1/3}O_2$. Universal but efficient, it can also be suitable to coat other layered cathode materials to ameliorate their electrochemical properties.

Keywords Cathode material · $LiNi_{1/3}Mn_{1/3}Co_{1/3}O_2$ · Surface coating · La_2O_3 particles · Outstanding cycling stability

Introduction

The demand for sustainable and clean energy, such as hydrogen, wind, wave, and solar energies, is becoming more and more critical owing to the fossil fuel crisis [1–6]. Electrochemical energy storage and conversion devices such as batteries and supercapacitors play an extremely important role in the fields of portable electronic products, electric vehicles, and smart electrical grids [7–11]. Therefore, systems of electrochemical energy storage and conversion such as Li-ion batteries (LIBs), lithium oxygen batteries, lithium-sulfur batteries, fuel cells, and supercapacitors are highly desired to meet the growing requirement for a multitude of emerging applications [12–20]. LIBs play an essential role in portable electronics, which are the crucial factor in the deployment of electric vehicles due to their high-energy density and long cycle life. Recently, the layered transition metal oxides ($Li[Ni_xCo_yMn_z]O_2$, nickel cobalt manganese (NCM), or NCM_{xyz}) cathode materials as potential candidates with high-power/energy densities and low cost and toxicity for replacing currently used $LiCoO_2$ in LIBs have been intensively investigated [21, 22]. Among those alternative layered transition metal oxides cathode materials, $LiNi_{1/3}Co_{1/3}Mn_{1/3}O_2$ (NCM) has been hotly studied owing to its superior cycle stability at low cutoff voltage, low cost, and simple preparation. However, there are still many problems that hinder its commercial application [23], such as (1) its high interfacial resistance after cycles and eventual capacity fading owing to the dissolution of transition metals into electrolyte mainly due to the reaction of electrode and electrolyte at the highly delithiated state; (2) its poor rate capability due to low electronic and ionic conductivity; and (3) Li/Ni cation mixing because of the similar radius of Li^+ (0.076 nm) and Ni^{2+} (0.069 nm).

Many effective measures have been used to address these problems. One of the most effective methods is doping with metal or non-metal which can improve the stability of the material structure. Some cations (Na [24], Mg [25], Mo [26], Ti [27], Al [28]) or anions (Cl [29], F [30]) doped in $LiNi_{1/3}Co_{1/3}Mn_{1/3}O_2$ cathode material on transition metal or oxygen sites had been certificated to improve the structure stability and electrochemical activity of $LiNi_{1/3}Co_{1/3}Mn_{1/3}O_2$ cathode materials without

Gang Sun and Chenxiao Jia contributed equally to this work.

✉ Guangjie Shao
shaoguangjie@ysu.edu.cn

✉ Xiujuan Qin
qinxj@ysu.edu.cn

[1] Hebei Key Laboratory of Applied Chemistry, College of Environmental and Chemical Engineering, Yanshan University, Qinhuangdao 066004, China

[2] State key Laboratory of Metastable Materials Science and Technology, Yanshan University, Qinhuangdao 066004, China

participating in the electrochemical reactions. The other effective strategy is surface modification by coating stable materials on electrodes which can protect the electrode surface from direct contact with the electrolyte and suppress the side reactions between the electrolyte and electrode. Wang et al. [31] demonstrated that Li_2ZrO_3 modification plays an important role to enhance the high-rate capability and cyclability of $LiNi_{1/3}Co_{1/3}Mn_{1/3}O_2$ at various working temperatures. Guo et al. [32] studied the enhancement of the electrochemical performance of $LiNi_{1/3}Co_{1/3}Mn_{1/3}O_2$ by MnO_2 modification, which indicated that the discharge capacity of MnO_2-coated samples was 155.15 mAh g^{-1}, while that of the pristine sample was 132.84 mAh g^{-1}. Zhang et al. [33] reported that surface modification of $LiNi_{1/3}Co_{1/3}Mn_{1/3}O_2$ with fluoroborate glass resulted in stable cyclability with capacity retention of 96.8% after 50 cycles while the capacity retention of bare one is 81.4%. Recently, some researchers have suggested that "trivalent oxides" (such as La_2O_3 [34, 35] and Al_2O_3 [36, 37]) are potential coating materials, compared to other materials, because these coating materials have the potential to prolong the cycle life of Li-ion batteries and surpass the performance of common coatings based on conventional materials [35]. In this work, the electrochemically inactive coating layer La_2O_3 has been introduced in cathode material, which can effectively prevent surface from interacting with acidic electrolyte components to suppress the side reactions and slow down the TM dissolutions. Though the electrochemical performance of electrodes were improved, the roles of coating materials are difficult to be clarified. Therefore, the roles of the metal oxide coating layer, especially in thin film cathode materials, are worthy of being studied.

In order to deeply research the effect of surface coating on structure and electrochemical performances of cathode material $LiNi_{1/3}Co_{1/3}Mn_{1/3}O_2$, herein, an uncontinuous La_2O_3-coated $LiNi_{1/3}Co_{1/3}Mn_{1/3}O_2$ has been successfully synthesized via a wet chemical process followed by a solid-state reaction at 800 °C for 5 h. And all the synthesized samples were galvanostatic charged and discharged in the voltage range of 2.5–4.5 V. The La_2O_3-modified $LiNi_{1/3}Mn_{1/3}Co_{1/3}O_2$ samples show earthshaking improved in cycle performance and rate capacity, which is attributed to the La_2O_3 layer that reduces electrochemical polarization and suppresses the side reactions between electrode and electrolyte. The structure and electrochemical performances of the La_2O_3-coated $LiNi_{1/3}Mn_{1/3}Co_{1/3}O_2$ were extensively investigated in this paper.

Experimental section

Materials preparation and characterization

Pristine $LiNi_{1/3}Mn_{1/3}Co_{1/3}O_2$ was provided by the 18th Research Institute Of China Electronics Technology Group Corporation. $LiNi_{1/3}Mn_{1/3}Co_{1/3}O_2$ was coated with the particles La_2O_3 via a solution-phase method. Stoichiometric amounts of the $LiNi_{1/3}Mn_{1/3}Co_{1/3}O_2$ powder and lanthanum nitrate ($La(NO_4)_3{\cdot}6H_2O$) were separately dissolved in absolute alcohol to obtain solution and the mass ratios of La/$LiNi_{1/3}Mn_{1/3}Co_{1/3}O_2$ were 0, 1, 3, and 5 wt% for three different samples, referred to as solution A. Urea as a precipitant was also dissolved in absolute alcohol, referred to as solution B. Then, solution B was gradually dropped into solution A with continuous stirring for 12 h under 80 °C. The precipitated hydroxide powder $La(OH)_3$-coated $LiNi_{1/3}Mn_{1/3}Co_{1/3}O_2$ was filtered off and dried at 120 °C overnight. The obtained powders were calcined at 800 °C for 5 h in air at a rate of 2 °C min^{-1} to get the La_2O_3-coated $LiNi_{1/3}Mn_{1/3}Co_{1/3}O_2$. The obtained compound was named as NCM, L-1, L-2, and L-3, respectively. In order to demonstrate that the material prepared via the above preparation process was La_2O_3 particles, we prepared the $LiNi_{1/3}Mn_{1/3}Co_{1/3}O_2$-free materials according to the above procedure.

The crystal structure of the samples was characterized by a Rigakud/MAX-2500/pc x-ray diffraction (XRD) with Cu Ka radiation at a scanning rate of 5° min^{-1}. The morphological characterizations of the powders were investigated with the Hitachi-S4800 scanning electronic microscope (SEM) and transmission electronic microscope (TEM) with model JEM2010.

Electrochemical measurements

A slurry coating procedure was adopted to prepare the working electrodes. The active material, carbon black as conductive agents, polyvinylidene fluoride (PVDF) as a binder with 80, 10, and 10 wt% mass fraction were dissolved in N-methyl-2-pyrrolidone (NMP) solvent. And then, the slurry was uniformly coated onto the aluminum foil and dried at 120 °C overnight and punched into discs of 10-mm diameter. The mass loading of active materials on the electrode should have an important influence on the electrochemical performances of the designed electrode [38–40], In this report, the mass loading of the active cathode materials on the aluminum foil is average 1.8 mg cm^{-2}. The electrochemical performance of the as-prepared sample was evaluated using CR2025-type coin cells with Li electrodes and electrolyte, which were assembled in an argon-filled glove box. The electrolyte employed was a solution of 1 M $LiPF_6$ in a mixture of ethylene carbonate and diethyl carbonate with 1:1 volume ratio. A microporous polypropylene film (Celgard 2400) was used as the separator. The cells were tested by galvanostatic charge-discharge cycling on a battery testing system (LAND, Wuhan, China) at 25 °C. The cyclic test was performed at 1C (1C = 200 mA g^{-1}) with cutoff potentials from 2.50~4.50 V. The rate levels for test were set as 0.2C, 0.5C, 1C, 2C, 5C, 10C, and 0.2C for 10 cycles each with the same potential range as the cyclic test. Electrochemical impedance spectroscopy (EIS)

measurements were performed in an alternating current frequency range from 1 mHz to 1 MHz using a CHI660E electrochemical workstation (Chenhua, Shanghai China) in the coin cell.

Result and discussion

The crystal structure of La_2O_3 powders, NCM, L-1, L-2, and L-3 was characterized by XRD, which can be shown in Fig. 1. From the XRD patterns of the obtained samples in Fig. 1, the diffraction peaks of NCM-free materials prepared by the above process are in accordance with those of La_2O_3 (JCPDS No. 05-0602), and no extra reflection peak of impurity phase is observed. The x-ray powder diffraction patterns of NCM, L-1, L-2, and L-3 powders exhibited a well-defined layer structure based on a hexagonal a-$NaFeO_2$ structure with an R-3 m space group and no impurity phases due to the low content of La_2O_3 phase. The distinct splitting of hexagonal doublets (006)/(012) and (018)/(110) peaks indicate an ordered layered structure [41]. There was no significant difference in the crystal structure before and after the coating, indicating the layered structure of $LiNi_{1/3}Mn_{1/3}Co_{1/3}O_2$ remained after the coating. Generally, the cation mixing, which is in consequence of Li/Ni site-exchange because of the similar radius of Li^+ (0.076 nm) and Ni^{2+} (0.069 nm), greatly influences the electrochemical performance, especially the capacity and cycling stability [42]. The Ni^{2+} ions in the Li layer, which decreased the d-spacing of Li layer in the ab planes due to the higher binding energy between the cation Ni and the anion O atom than between the cation Li and the anion O atom, not only decreased discharge capacity but also impeded to Li^+ ionic diffusivity [43, 44]. Moreover, the intensity ratio of I(003)/I(104) is a reliable indicator for determining the

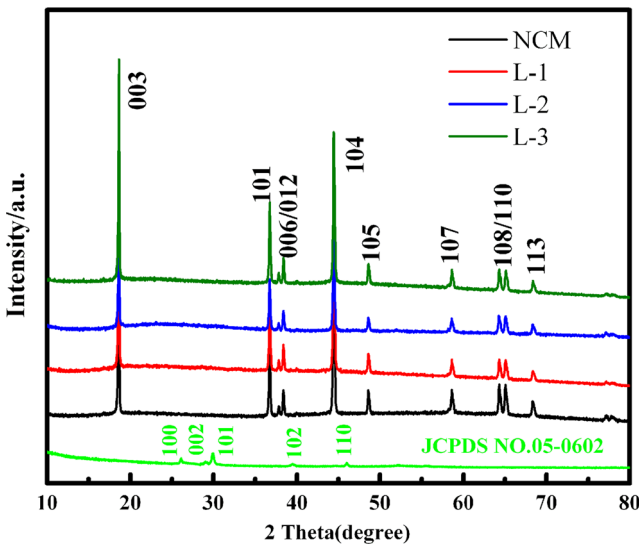

Fig. 1 XRD patterns of NCM, L-1, L-2, L-3, and La_2O_3

cation distribution in the lattice of layered oxides [45, 46], and the value of 1.2 is supposed to be the boundary of cation disordering, and the higher value means better ordering for the cations. The value of I(003)/I(104) for NCM, L-1, L-2, and L-3 samples is 1.138, 1.408, 1.521, and 1.414, respectively. This result indicates that the L-2 sample exhibits the best layered structure and the lowest cation mixing which can facilitate the diffusion of lithium ions. Therefore, the lower cation mixing in La_2O_3-coated $LiNi_{1/3}Mn_{1/3}Co_{1/3}O_2$ samples infer a better electrochemical performance.

To explore the influence of the coatings on surface morphology, SEM and TEM were used to analyze the surface morphologies and microstructures of bare and the La_2O_3-coated $LiNi_{1/3}Mn_{1/3}Co_{1/3}O_2$ samples. As shown in Fig. 2a–d, the SEM images exhibit morphology change of NCM (a), L-1 (b), L-2 (c), and L-3 (d) samples. The primary particle size of the bare and coated $LiNi_{1/3}Mn_{1/3}Co_{1/3}O_2$ samples were distributed with a particle size ranging from 1 to 2 μm and displayed a smooth surface and clear boundary, while the surface-coated $LiNi_{1/3}Mn_{1/3}Co_{1/3}O_2$ was distinctly covered by La_2O_3 particle with a particle size ranging from 10 to 50 nm. It can form an uncontinuous La_2O_3 coating layer on the surface of the cathode materials due to uneven particle dispersion and small coating amount. As the coating amount increases, the surface of the particles become rough and form a dense coating layer. The elemental distribution of O, Ni, Co, Mn, and La of the L-3 composite was analyzed by EDS mapping. From Fig. 2e, f, it is shown that elements O, Ni, Co, Mn, and La are uniformly distributed in the sample. SEM image and element mapping of L-3 particles (Fig. 2e, f) revealed that La was successfully coated on the surface of $LiNi_{1/3}Mn_{1/3}Co_{1/3}O_2$ cathode material. Figure 3 shows TEM images of the NCM, L-1, L-2, and L-3 samples. The uncoated sample displayed a smooth surface compared to the coated samples. The surface of the coating material is relatively coarse. When the content of coating is too low, the surface coating layer of the material is incomplete. The coating layer appears as small particles adsorbed on the surface of the $LiNi_{1/3}Mn_{1/3}Co_{1/3}O_2$ cathode material. As the coating content increases, the size of particles increases and the coating layer becomes complete and thicker. Thus, from the analyses of the XRD, SEM, TEM, and EDS patterns, we can come to the conclusion that the La_2O_3 successfully coated on the surface of L-1, L-2, and L-3 samples.

The galvanostatic charge-discharge tests have been performed to compare the electrochemical performance of pristine $LiNi_{1/3}Co_{1/3}Mn_{1/3}O_2$ and La_2O_3-modified $LiNi_{1/3}Co_{1/3}Mn_{1/3}O_2$. The charge-discharge capacity profiles at different cycles (1st, 10th, 20th, 30th, 40th, 50th, 60th, 70th, 80th, 90th, and 100th) of the pristine and L-2 electrode at 1.0C in the voltage range of 2.5–4.5 V versus Li are shown in Fig. 4a, b, respectively. There is only one voltage plateau at 3.5–3.8 V observed for the as-synthesized materials in the cycle corresponding to the redox activity of the transition metal cations,

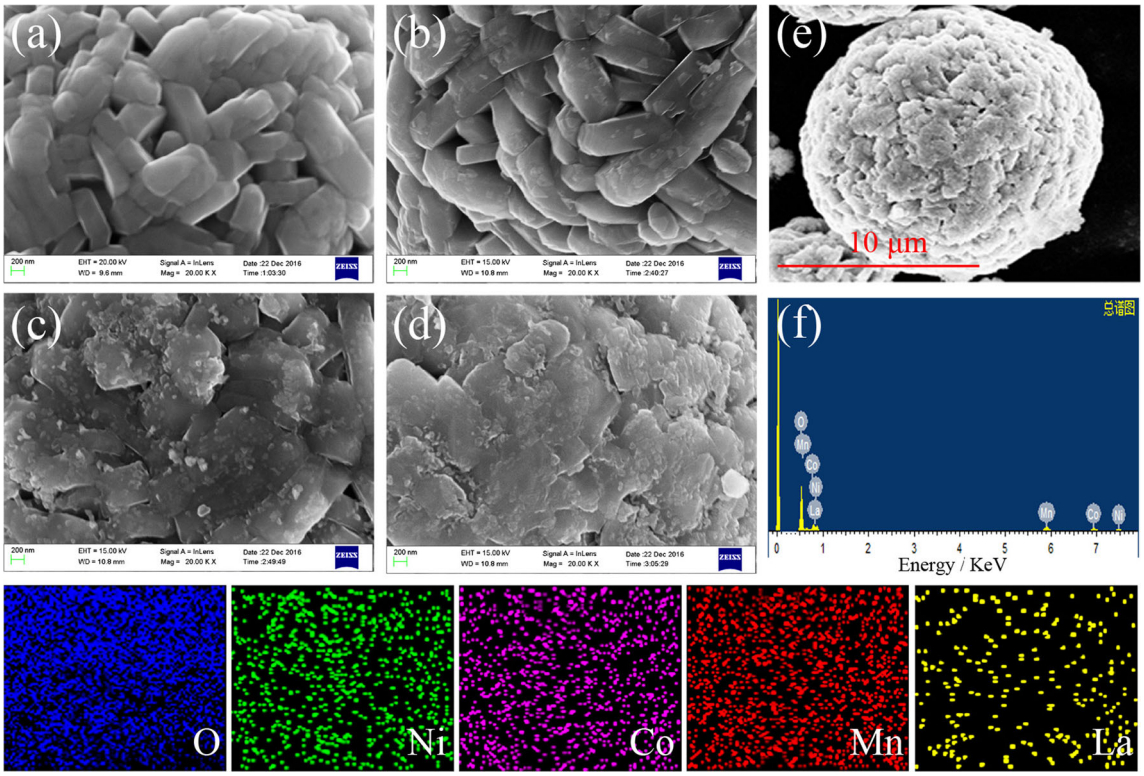

Fig. 2 SEM images for **a** NCM, **b** L-1, **c** L-2, and **d** L-3. **e–f** EDS mapping images for L-2 sample

namely, Ni, with typical layer-structured $LiNi_{1/3}Co_{1/3}Mn_{1/3}O_2$. Before the rapid drop at about 3.5 V in the discharge curves, voltage decrease of the L-2 electrode (in Fig. 4b) is quite smooth compared with the pristine electrode (in Fig. 4a), and the platforms of charge and discharge curves for L-2 electrode are longer than pristine electrode, indicating a higher

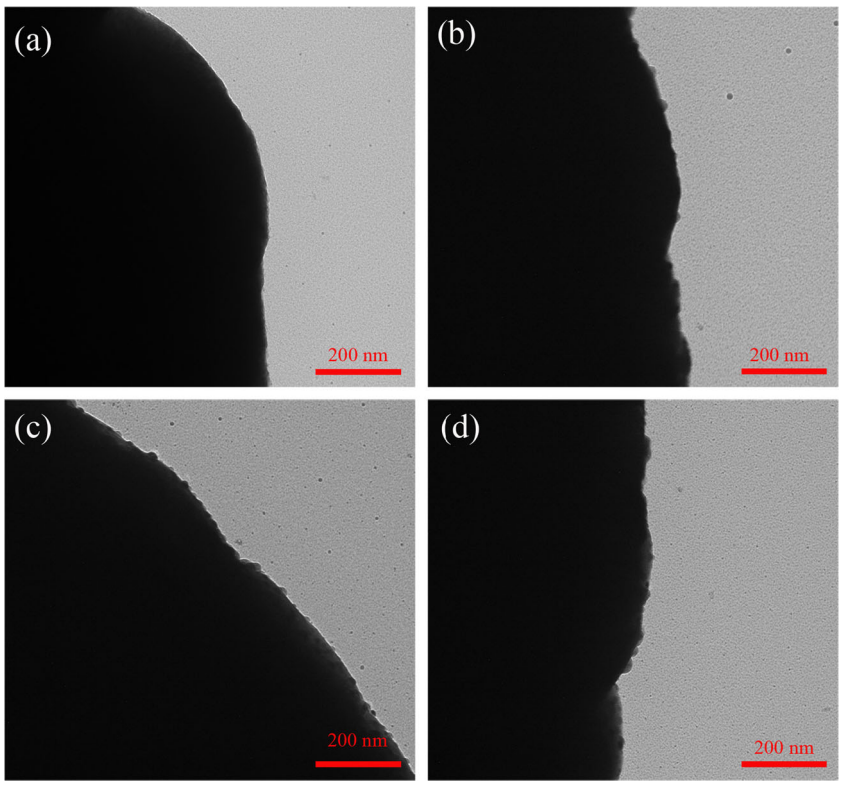

Fig. 3 TEM images for **a** NCM, **b** L-1, **c** L-2, and **d** L-3

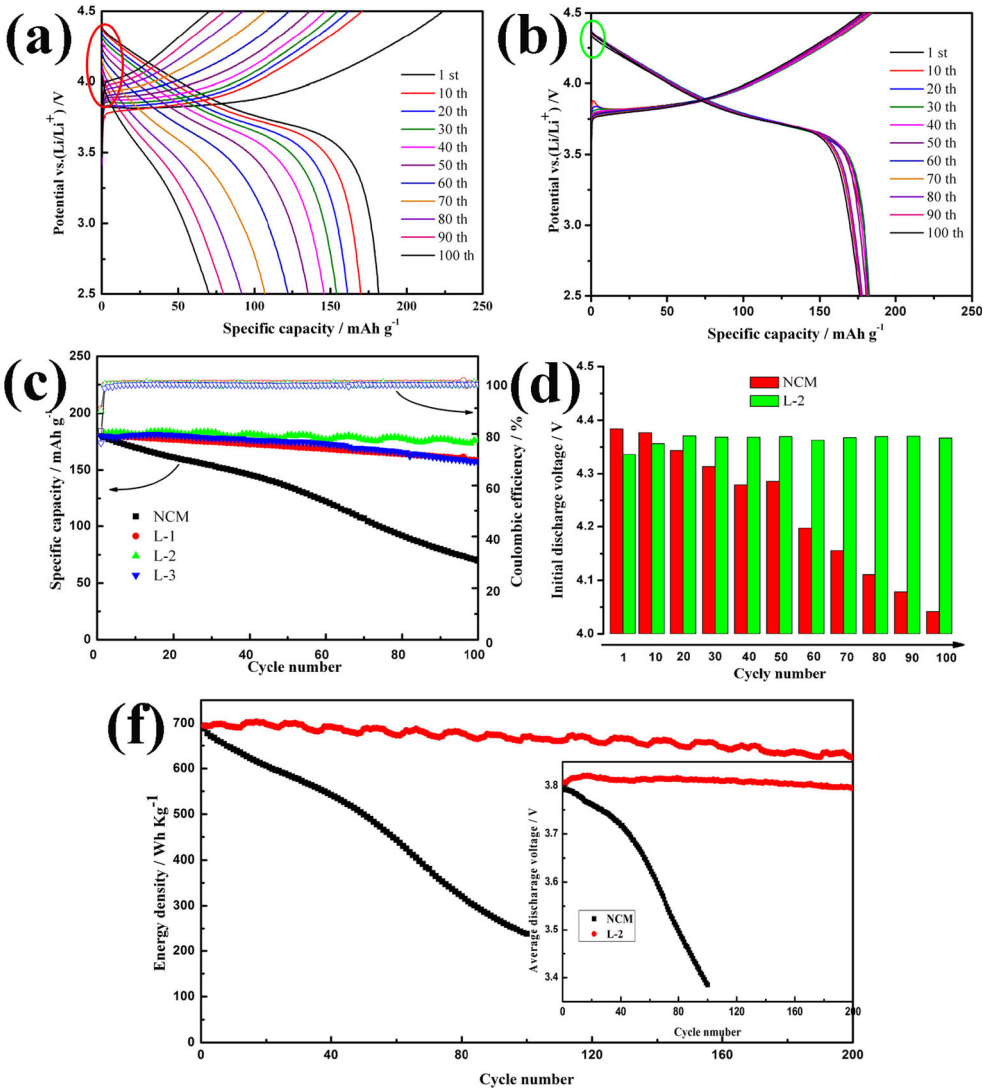

Fig. 4 The charge-discharge curves of the NCM (**a**) and L-2 (**b**) electrodes. **c** Plots of the discharge capacity with the Coulombic efficiency versus cycle number for as-prepared electrodes. **d** The initial discharge voltage of the NCM and L-2 electrodes (IR drop). **f** Energy densities and average discharge voltage (illustration) versus cycle number plots at 1 C of NMC and L-2 materials. Those electrodes measured at a 1C rate in the potential range of 2.5–4.5 V versus Li

energy density and a great cycling stability. Notably, the pristine electrode suffers from observable capacity/voltage fading. The dissolution of transition metal ions might take place upon long cycles, along with the crystal destruction and the decomposition of electrolyte, leading to severe performance decay. Figure 4c shows the specific capacity and Coulombic efficiency of the NCM, L-1, L-2, and L-3 electrodes at 1C rate between 2.5 and 4.5 V are plotted versus cycle number. The cycling data of the electrodes are listed in Table 1. A significant difference was found in the field of the capacity retention; the capacity retention of cathodes was hugely improved after surface modification. The initial specific capacities of the NCM, L-1, L-2, and L-3 electrodes were found to be 181.6, 181.0, 181.3, and 179.9 mA h g^{-1}, respectively. And the capacity retentions of the NCM, L-1, L-2, and L-3 electrodes are 38.6, 87.6, 96.1, and 87.1% over 100 cycles, respectively. Obviously, surface coating of La_2O_3 can greatly enhance the cycle performance of the $LiNi_{1/3}Mn_{1/3}Co_{1/3}O_2$ material. The L-2 electrode possesses the highest discharge capacity after 100 cycles and that means the best cycling stability for the modified sample. The good cycling stability of the surface-modified samples was due to the presence of coating layer, which protected the bulk material from being corroded by electrolyte and suppressed the electrolyte decomposition during cycling. The IR-drops for the NCM and L-2 electrodes of the 1st, 10th, 20th, 30th, 40th, 50th, 60th, 70th, 80th, 90th, and 100th cycle are presented in Fig. 4d. It is known that LIB cathodes suffer from the effect of polarization, which leads to the open-circuit voltage decay and thus the starting discharge voltage is usually lower than 4.5 V [47]. The reducing value in voltage is a criterion for evaluating the effect of polarization [48]. As can be seen from the IR drop in Fig. 4d, the pristine electrode shows an initial IR drop from 4.5 to 4.38 V, which then decrease to 4.04 V after 100 cycles gradually. In comparison, the IR drop of L-2 electrode is almost stabilized at 4.4 V in 100 cycles. This implies a larger polarization for the pristine electrode. The energy densities and average discharge voltage (illustration) versus cycle number plots at 1C of NMC

Table 1 Cycling performance of the NCM, L-1, L-2, and L-3 electrodes

	1st discharge capacity (mA h g^{-1})	100th discharge capacity (mA h g^{-1})	100th capacity retention (%)	Voltage decay (mV)	Energy retention (%)
NCM	181.6	70.2	38.6	407 (100th)	34.5 (100th)
L-1	181.0	158.5	87.6	/	/
L-2	181.3	174.3	96.1	10.3 (100th) 26.9 (200th)	96.5 (100th) 89.7 (200th)
L-3	179.9	156.7	87.1	/	/

and L-2 materials are shown in Fig. 4f and Table 1. The decrements of the average discharge voltages for L-2 electrode is 10.3 mV over 100th cycle and 26.9 mV over 200th cycle compared to 407 mV over 100th cycle for bare NCM. The continuous phase transformation from the layered to spinel structure during the charge-discharge process may result in the voltage decay, as shown in previous reports [49, 50]. The energy densities of the NCM and L-2 electrode are 688.65 and 694.80 Wh kg^{-1}, respectively. And the energy densities retention of L-2 is 96.5% after 100 cycles and 89.7% after 200 cycles compared to 34.5% after 100 cycles for bare NCM. The L-2 electrode displays capacity and voltage stability obviously better than those of the NCM electrode. All these results indicate that La_2O_3 coating on NCM material can effectively reduce the polarization of the material, enhance cycle stability, and effectively suppress voltage and energy attenuation.

To further evaluate the electrochemical properties of the as-prepared cathodes, the rate capabilities were tested in the range of 2.5–4.5 V at various current densities and the discharge curves at various rates, as shown in Fig. 5. As expected, the specific capacities of all cathodes decrease with an increase in the current density due to the increasing polarization and L-2 electrode exhibits a best rate capability than other electrodes. The discharge capacity of NCM cathode material is 189.0, 172.7, 158.4, 140.3, 115.8, and 86.9 mAh g^{-1} at 0.2C, 0.5C, 1C, 2C, 3C, and 5C, respectively. While the L-2 cathode material offers the discharge capacity of about 187.0, 182.0, 171.2, 157.2, 146.8, and 137.5 mAh g^{-1} at the same rates, respectively. From Fig. 5a, it can be seen that when the

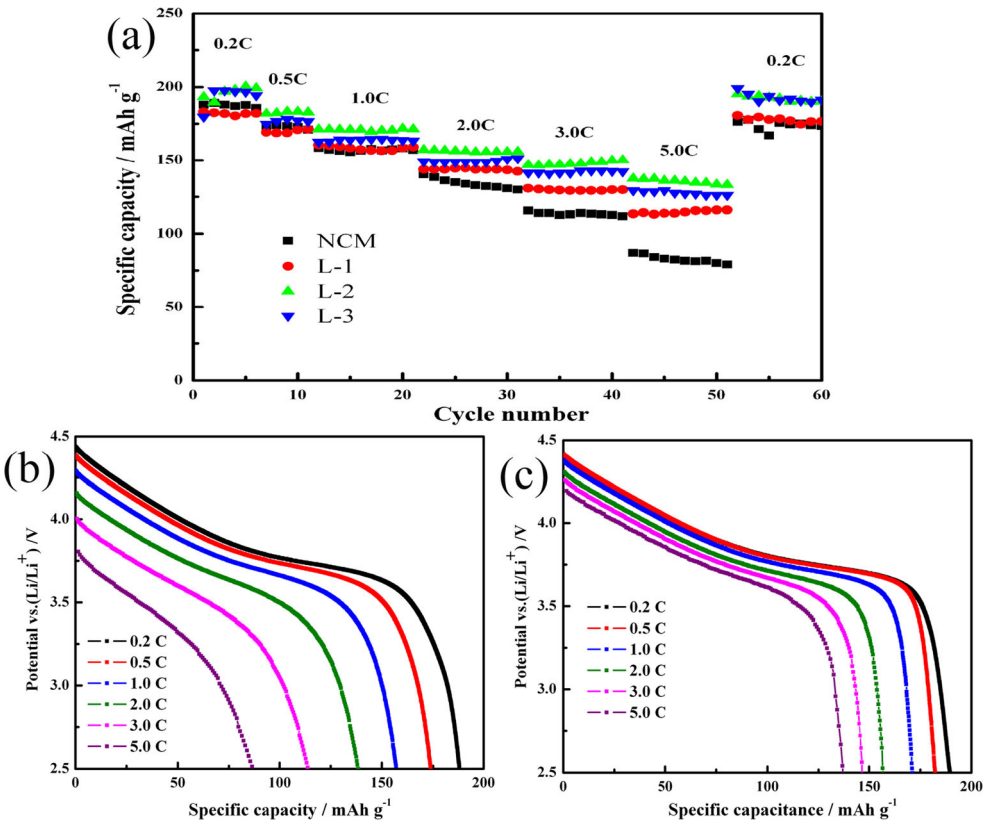

Fig. 5 **a** Rate capability tests at several currents (C rates) for NCM, L-1, L-2, and L-3 electrodes in the potential range of 2.5–4.5 V versus Li. Discharge profiles of NCM (**b**) and L-2 (**c**) electrodes cathode at various C rates of 0.2, 0.5, 1, 2, 3, and 5

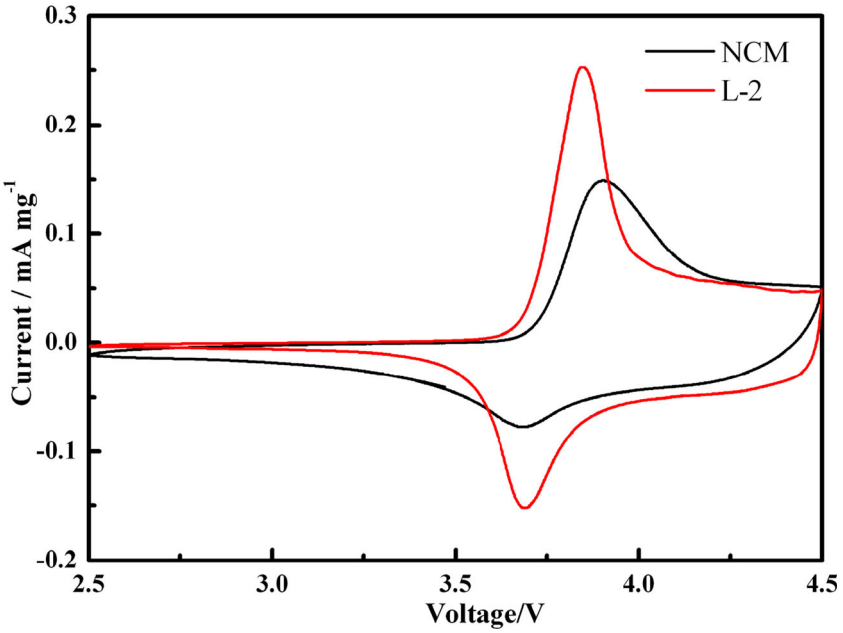

Fig. 6 Cyclic voltammetry data for NCM and L-2 electrode after 100th cycle and voltage range from 2.5 to 4.5 V

current density was increased to high rate, the significant differences can be observed clearly. The pristine NCM shows severe capacity degradation as the rate increases from 0.2C to 5C. In comparison, L-2 electrode exhibits much better rate capability, suggesting better structural stability of the coated sample for rapid Li^+ insertion/extraction. Figure 5b, c show the discharge curves at different C rates. One of the most important reasons, which result in dramatically reduction of the working voltage at rates of 0.2C and 5C for the pristine NCM, is the undesirable increased interphase resistances caused by the side reaction on the interface between electrode and electrolytes [51]. In comparison, the voltage fading and capacity loss are obviously restrained in L-2 electrode.

To further analyze the electrochemical nature of pristine and L-2 electrodes, CV measurements were conducted at voltages between 2.5 and 4.5 V at a scan rate of 0.1 mV s^{-1}. The CV curves of all electrodes after 100th cycle are illustrated in Fig. 6. There is a pair of oxidation and reduction peaks in every curve, which corresponds to Ni^{2+}/Ni^{4+} redox couple [52]. As shown in Fig. 6, their anodic peaks are 3.908 and 3.842 V, reduction peaks are 3.681 and 3.698 V, and their redox reaction gaps can be calculated to be 0.23 and 0.144 V, respectively, indicating that the polarization of the sample L-2 is small compared with the pristine samples. The above results suggest that the sample L-2 has the best electrochemical performance than others.

Figure 7a shows the Nyquist plots of NCM and L-2 electrode after 100th cycling. The Nyquist plots are fitted and presented in Fig. 7b, in the medium frequency region, a semicircle can be found, which is related to the charge-transfer resistance of the electrode. A line at low-frequency region with about 45° to the real axis is assigned to the Li^+ diffusion within the electrode [53]. In the equivalent circuits inserted in Fig. 7b, Rs represents the solution resistance, which includes the ohmic resistance in NCM or L-2 materials and the tab of cathode/anode. Re represents the diffusion resistance of Li^+ in the surface layer (including SEI film). The parameter Rct corresponds to the charge-transfer resistance, CPE1 refer to the nonideal capacitance of the surface layer, and CPE2 is assigned to charge-transfer capacitance, Zw refers to the

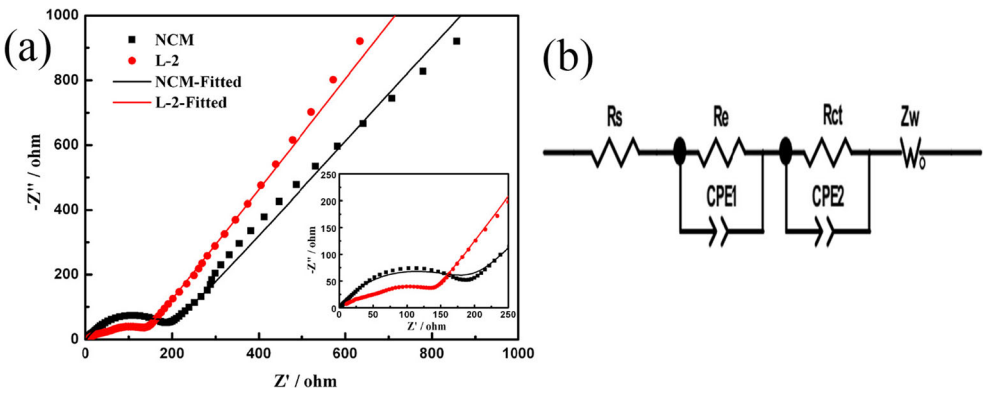

Fig. 7 **a** Fitted Nyquist plots for NCM and L-2 electrode after 100th cycle. **b** The corresponding equivalent circuits for NCM and L-2 electrode

Table 2 Electrochemical impedance of the NCM and L-2 electrodes

Sample	Rs	Re	Rct
NCM-0	2.556	13.19	149.6
NCM-5	3.068	72.83	54.01

Warburg impedance, which represents the diffusion behavior of Li^+ in the bulk [54]. The simulated values after the 100th cycle are shown in Table 2; the resistances of L-2 are lower than that of NCM, implying a better high rate performance in L-2 than NCM. From Fig. 7, it can be seen that La_2O_3-coated $LiNi_{1/3}Mn_{1/3}Co_{1/3}O_2$ material could form an SEI film to protect the NCM electrode after 100 cycles. The Rct of NCM and L-2 according to the fitting results were 149.6 and 54.01 Ω, respectively, indicating the improved electronic contact and more effective charge transport of L-2 compared with NCM, which was in accordance with difference of the sizes of the two semicircles. It indicates that a protective layer has been formed on the surface of the cathode materials during cycles, which can reduce the degradation of material structure and effectively improved the electrochemical kinetics of the material.

Conclusion

High-voltage layered $LiNi_{1/3}Mn_{1/3}Co_{1/3}O_2$ oxides, which can deliver high-energy density, are highly desired for next-generation energy storage devices and capable of addressing some of the challenges associated. However, the cathode material suffers from severe voltage and capacity attenuation at high cutoff voltage due to the structure instability and side reaction between electrode and electrolyte at the highly delithiated state. To improve the high voltage stability and high-energy density of the cathode material, an uncontinuous La_2O_3-coated $LiNi_{1/3}Mn_{1/3}Co_{1/3}O_2$ has been synthesized via a wet chemical process followed by a solid state reaction at 800 °C for 5 h. It can be observed from the XRD patterns and SEM and TEM images that the La_2O_3-coated $LiNi_{1/3}Mn_{1/3}Co_{1/3}O_2$ samples with uncontinuous La_2O_3 coating showed no change in the structure and morphology as compared to pristine NCM. La_2O_3-coated $LiNi_{1/3}Mn_{1/3}Co_{1/3}O_2$ samples show greatly elevated discharge capacity, energy density, and rate capacity due to the protective role of the La_2O_3 layer, which suppresses the side reactions between electrode and electrolyte, effectively slows down the voltage decay, and reduces electrochemical polarization during cycling of $LiNi_{1/3}Mn_{1/3}Co_{1/3}O_2$. Through the surface modification method, 3 wt% La_2O_3-coated $LiNi_{1/3}Mn_{1/3}Co_{1/3}O_2$ illustrated highest rate capability, lowest voltage decay, outstanding cycling performance, and excellent energy density, which attribute to a protective layer that has been formed on the surface of the cathode materials during the cycles. The discharge capacity of NCM at a 5C rate increases from 86.9 to 137.5 mA h g^{-1} upon coating with La_2O_3. Furthermore, the layer stability of $LiNi_{1/3}Mn_{1/3}Co_{1/3}O_2$ has been enhanced after La_2O_3 coating, which results in improved midpoint voltages. The capacity retention of 3 wt% La_2O_3-coated $LiNi_{1/3}Mn_{1/3}Co_{1/3}O_2$ is 96.1% after 100 cycles compared to 38.6% after 100 cycles for bare NCM. The decrements of the average discharge voltages for 3 wt% La_2O_3-coated $LiNi_{1/3}Mn_{1/3}Co_{1/3}O_2$ electrode is 10.3 mV over 100th cycle and 26.9 mV over 200th cycles compared to 407 mV over 100th cycle for bare NCM. And the energy densities retention of 3 wt% La_2O_3-coated $LiNi_{1/3}Mn_{1/3}Co_{1/3}O_2$ electrode is 96.5% after 100 cycles and 89.7% after 200 cycles compared to 34.5% after 100 cycles for bare NCM. All the above results show that the surface coating of $LiNi_{1/3}Co_{1/3}Mn_{1/3}O_2$ with La_2O_3 is an effective way to improve its electrochemical performance.

Funding information The authors are grateful for the financial support from the National Natural Science Foundation of China (nos. 51674221 and 51704261) and the Natural Science Foundation of Hebei Province (B2018203330 and B2018203360).

Compliance with ethical standards

Conflicts of interest There are no conflicts to declare.

References

1. Tarascon JM, Armand M (2001) Issues and challenges facing rechargeable lithium batteries. Nature 414:359–367
2. Ibrahim H, Ilinca A, Perron J (2008) Energy storage systems—characteristics and comparisons. Renew Sustain Energy Rev 12:1221–1250
3. Yin X, Sun G, Wang L, Bai L, Su L, Wang Y, Du Q, Shao G (2017) 3D hierarchical network NiCo2S4 nanoflakes grown on Ni foam as efficient bifunctional electrocatalysts for both hydrogen and oxygen evolution reaction in alkaline solution. Int J Hydrog Energy 42:25267–25276
4. Yang W, Yang W, Song A, Gao L, Sun G, Shao G (2017) Pyrrole as a promising electrolyte additive to trap polysulfides for lithium-sulfur batteries. J Power Sources 348:175–182
5. Seh ZW, Sun Y, Zhang Q, Cui Y (2016) Designing high-energy lithium-sulfur batteries. Chem Soc Rev 45:5605–5634
6. Su L, Gao L, Du Q, Hou L, Ma Z, Qin X, Shao G (2018) Construction of NiCo2O4@MnO2 nanosheet arrays for high-performance supercapacitor: highly cross-linked porous heterostructure and worthy electrochemical double-layer capacitance contribution. J Alloys Compd 749:900–908. https://doi.org/10.1016/j.jallcom.2018.03.353
7. Ma Z, Shao G, Fan Y, Wang G, Song J, Shen D (2016) Construction of hierarchical α-MnO2 nanowires@ ultrathin δ-MnO2 nanosheets core-shell nanostructure with excellent cycling stability for high-power asymmetric supercapacitor electrodes. ACS Appl Mater Interfaces 8:9050–9058
8. Song A, Cao L, Yang W, Li Y, Qin X, Shao G (2018) Uniform multilayer graphene-coated Iron and Iron-carbide as oxygen reduction catalyst. ACS Sustain Chem Eng 6:4890–4898. https://doi.org/10.1021/acssuschemeng.7b04319

9. Du Q, Su L, Hou L, Sun G, Feng M, Yin X, Ma Z, Shao G, Gao W (2018) Rationally designed ultrathin Ni-Al layered double hydroxide and graphene heterostructure for high-performance asymmetric supercapacitor. J Alloys Compd 740:1051–1059
10. Yang W, Yang W, Song A, Sun G, Shao G (2018) 3D interconnected porous carbon nanosheets/carbon nanotubes as a polysulfide reservoir for high performance lithium-sulfur batteries. Nanoscale 10:816–824
11. Wang J, Li Y, Sun X (2013) Challenges and opportunities of nanostructured materials for aprotic rechargeable lithium–air batteries. Nano Energy 2:443–467
12. Armand M, Tarascon JM (2008) Building better batteries. Nature 451:652–657
13. Yu FD, Que LF, Wang ZB, Xue Y, Zhang Y, Liu BS, Gu DM (2017) Controllable synthesis of hierarchical ball-in-ball hollow microspheres for a high performance layered Li-rich oxide cathode material. J Mater Chem A 5:9365–9376
14. Chen Z, Ma Z, Song J, Wang L, Shao G (2016) Novel one-step synthesis of wool-ball-like Ni-carbon nanotubes composite cathodes with favorable electrocatalytic activity for hydrogen evolution reaction in alkaline solution. J Power Sources 324:86–96
15. Song J, Xing R, Jiao T, Peng Q, Yuan C, Möhwald H, Yan X (2018) Crystalline dipeptide nanobelts based on solid–solid phase transformation self-assembly and their polarization imaging of cells. ACS Appl Mater Interfaces 10:2368–2376
16. Li Y, Wang L, Song A, Xia M, Li Z, Shao G (2018) The study on the active origin of electrocatalytic water splitting using Ni-MoS2 as example. Electrochim Acta 268:268–275
17. Yang W, Yang W, Kong L, Song A, Qin X, Shao G (2018) Phosphorus-doped 3D hierarchical porous carbon for high-performance supercapacitors: a balanced strategy for pore structure and chemical composition. Carbon 127:557–567
18. Zhang Q, Li Y, Phanlavong P, Wang Z, Jiao T, Qiu H, Peng Q (2017) Highly efficient and rapid fluoride scavenger using an acid/base tolerant zirconium phosphate nanoflake: behavior and mechanism. J Clean Prod 161:317–326
19. Kwabi DG, Ortiz-Vitoriano N, Freunberger SA, Chen Y, Imanishi N, Bruce PG, Shao-Horn Y (2014) Materials challenges in rechargeable lithium-air batteries. MRS Bull 39:443–452
20. Manthiram A, Song B, Li W (2017) A perspective on nickel-rich layered oxide cathodes for lithium-ion batteries. Energy Storage Materials 6:125–139
21. Choi NS, Chen Z, Freunberger SA, Ji X, Sun YK, Amine K, Yushin G, Nazar LF, Cho J, Bruce PG (2012) Challenges facing lithium batteries and electrical double-layer capacitors. Angew Chem Int Ed 51:9994–10024
22. Li Y, Wu C, Bai Y, Liu L, Wang H, Wu F, Zhang N, Zou Y (2016) Hierarchical mesoporous lithium-rich Li[Li0.2Ni0.2Mn0.6]O2 cathode material synthesized via ice templating for lithium-ion battery. ACS Appl Mater Interfaces 8:18832
23. Sun G, Yin X, Yang W, Zhang J, Du Q, Ma Z, Shao G, Wang Z-B (2018) Synergistic effects of ion doping and surface-modifying for lithium transition-metal oxide: synthesis and characterization of La2O3-modified LiNi1/3Co1/3Mn1/3O2. Electrochim Acta 272:11–21
24. Li Y, Liu J, Lei Y, Lai C, Xu Q (2017) Enhanced electrochemical performances of Na-doped cathode material LiNi1/3Co1/3Mn1/3O2 for lithium-ion batteries. J Mater Sci 52:13596–13605
25. Li JB, Xu YL, Xiong LL, Wang JP (2011) Improvement of LiNi1/3Co1/3Mn1/3O2 cathode materials by nano-MgO doping. Acta Phys -Chim Sin 27(2597):2593–2599
26. Zhang Y, Wang Z-B, Yu F-D, Que L-F, Wang M-J, Xia Y-F, Xue Y, Wu J (2017) Studies on stability and capacity for long-life cycle performance of Li(Ni0.5Co0.2Mn0.3)O2 by Mo modification for lithium-ion battery. J Power Sources 358:1–12
27. Li G, Huang Z, Zuo Z, Zhang Z, Zhou H (2015) Understanding the trace Ti surface doping on promoting the low temperature performance of LiNi 1/3 co 1/3 Mn 1/3 O 2 cathode. J Power Sources 281:69–76
28. Hu Z, Deng Z, Wei Q, Zhao T, Wang Y, Yu Z, Ma L, Zhou K (2017) Roles of Al-doped ZnO (AZO) modification layer on improving electrochemical performance of LiNi 1/3 Co 1/3 Mn 1/3 O 2 thin film cathode. Ionics 1–12
29. Zhang H L, Liu S (2013) Synthesis and characterization of LiNi1/3Co1/3Mn1/3O2?xClx as cathode materials for Lithium ion batteries at 55°C. Adv Mater Sci Eng (2013-12-23) 2013: in press
30. Kim C, Yang SB, Yoo GW, Son JT (2016) F-doped 0.5Li2MnO3·0.5LiNi1/3Co1/3Mn1/3O2 high porous nanofibers as cathode material for lithium-ion battery. J Nanosci Nanotechnol 16:8342–8346
31. Wang C, Chen L, Zhang H, Yang Y, Wang F (2014) Li2ZrO3 coated LiNi1/3Co1/3Mn1/3O2 for high performance cathode material in lithium batteries. Electrochim Acta 119:236–242
32. Guo X, Cong LN, Zhao Q, Tai LH, Wu XL, Zhang JP, Wang RS, Xie HM, Sun LQ (2015) Enhancement of electrochemical performance of LiNi 1/3 Co 1/3 Mn 1/3 O 2 by surface modification with MnO 2. J Alloys Compd 651:12–18
33. Zhang Q, Wang L, Zhu C, Sun Z, Cheng W, Lv D, Ren W, Bian L, Xu J, Chang A (2017) Enhanced electrochemical capability of LiNi1/3Co1/3Mn1/3O2 cathode materials coated with fluoroborate glass for lithium-lon batteries. Chemelectrochem 4:1199–1204
34. Aykol M, Kirklin S, Wolverton C (2015) Thermodynamic aspects of cathode coatings for Lithium-ion batteries. Adv Energy Mater 4
35. Aykol M, Kim S, Hegde VI, Snydacker D, Lu Z, Hao S, Kirklin S, Morgan D, Wolverton C (2016) High-throughput computational design of cathode coatings for li-ion batteries. Nat Commun 7: 13779
36. Du K, Xie H, Hu G, Peng Z, Cao Y, Yu F (2016) Enhancing the thermal and upper voltage performance of Ni-rich cathode material by a homogeneous and facile coating method: spray-drying-coating nano-Al2O3. ACS Appl Mater Interfaces 8: 17713, 17720
37. Huang Y, Chen J, Cheng F, Wan W, Liu W, Zhou H, Zhang X (2010) A modified Al2O3 coating process to enhance the electrochemical performance of Li(Ni1/3Co1/3Mn1/3)O2 and its comparison with traditional Al2O3 coating process. J Power Sources 195: 8267–8274
38. Wang B, Abdulla WA, Wang D, Zhao XS (2015) A three-dimensional porous LiFePO cathode material modified with a nitrogen-doped graphene aerogel for high-power lithium ion batteries. Energy Environ Sci 8:869–875
39. Yi TF, Mei J, Zhu YR (2016) Key strategies for enhancing the cycling stability and rate capacity of LiNi0.5Mn1.5O4 as high-voltage cathode materials for high power lithium-ion batteries. J Power Sources 316:85–105
40. Yi T-F, Li Y-M, Yang S-Y, Zhu Y-R, Xie Y (2016) Improved cycling stability and fast charge-discharge performance of cobalt-free lithium-rich oxides by magnesium-doping. ACS Appl Mater Interfaces 8:32349–32359
41. Ren D, Shen Y, Yang Y, Shen L, Levin B, Yu Y, Muller D A, Abruña H D (2017) Systematic optimization of battery materials: key parameter optimization for the scalable synthesis of uniform, high-energy and high stability LiNi0.6Mn0.2Co0.2O2 cathode material for lithium-ion batteries. ACS Appl Mater Interfaces
42. Zhang X, Jiang WJ, Mauger A, Qilu GF, Julien CM (2011) Minimization of the cation mixing in Li 1+x (NMC) 1−xO2 as cathode material. J Power Sources 195:1292–1301
43. Lee J, Urban A, Li X, Su D, Hautier G, Ceder G (2014) Unlocking the potential of cation-disordered oxides for rechargeable lithium batteries. Science 343:519–522
44. Liu W, Oh P, Liu X, Lee MJ, Cho W, Chae S, Kim Y, Cho J (2015) Nickel-rich layered lithium transition-metal oxide for high-energy lithium-ion batteries. Angew Chem Int Ed 54:4440–4457

45. Yin K, Fang W, Zhong B, Guo X, Tang Y, Nie X (2012) The effects of precipitant agent on structure and performance of LiNi 1/3 co 1/3 Mn 1/3 O 2 cathode material via a carbonate co-precipitation method. Electrochim Acta 85:99–103
46. Yao L, Yao H, Xi G, Feng Y (2016) Recycling and synthesis of LiNi1/3Co1/3Mn1/3O2 from waste lithium ion batteries using D,L-malic acid. RSC Adv 6:1833–1840
47. Bian X, Fu Q, Pang Q, Gao Y, Wei Y, Zou B, Du F, Chen G (2016) Multi-functional surface engineering for Li-excess layered cathode material targeting excellent electrochemical and thermal safety properties. ACS Appl Mater Interfaces 8:3308–3318
48. Li Q, Li G, Fu C, Luo D, Fan J, Li L (2014) K(+)-doped Li(1.2)Mn(0.54)Co(0.13)Ni(0.13)O2: a novel cathode material with an enhanced cycling stability for lithium-ion batteries. ACS Appl Mater Interfaces 6:10330
49. Nayak PK, Grinblat J, Levi M, Levi E, Kim S, Choi JW, Aurbach D (2016) Al doping for mitigating the capacity fading and voltage decay of layered Li and Mn-rich cathodes for li-ion batteries. Adv Energy Mater 6:1502398
50. Sun G, Yin X, Yang W, Song A, Jia C, Yang W, Du Q, Ma Z, Shao G (2017) The effect of cation mixing controlled by thermal treatment duration on the electrochemical stability of lithium transition-metal oxides. Phys Chem Chem Phys 19:29886–29894
51. He M, Su CC, Peebles C, Feng Z, Connell JG, Liao C, Wang Y, Shkrob IA, Zhang Z (2016) Mechanistic insight in the function of phosphite additives for protection of LiNi0.5Co0.2Mn0.3O2 cathode in high voltage li-ion cells. ACS Appl Mater Interfaces 8: 11450–11458
52. He R, Zhang L, Yan M, Gao Y, Liu Z (2016) Effects of Cr2O3-modified LiNi1/3Co1/3Mn1/3O2 cathode materials on the electrochemical performance of lithium-ion batteries. J Mater Sci 52:1–9
53. Yang C, Zhang X, Huang J, Ao P, Zhang G (2016) Enhanced rate capability and cycling stability of Li 1.2-x Na x Mn 0.54 co 0.13 Ni 0.13 O 2. Electrochim Acta 196:261–269
54. Wang L, Zhao J, He X, Gao J, Li J, Wan C, Jiang C (2012) Electrochemical impedance spectroscopy (EIS) study of LiNi1/3Co1/3Mn1/3O2 for Li-ion batteries. Int J Electrochem Sci 7: 345–353